Title

PHOTOPEAK METHOD FOR THE COMPUTER ANALYSIS OF GAMMA-RAY SPECTRA FROM SEMICONDUCTOR DETECTORS

Authors

Routti, Jorma T.
Prussin, Stanley G.

Publication Date

1968-12-01

UCRL-17672
ey. 2

PHOTOPEAK METHOD FOR THE COMPUTER ANALYSIS OF GAMMA-RAY SPECTRA FROM SEMICONDUCTOR DETECTORS

Jorma T. Routti and Stanley G. Prussin

December 1, 1968

LAWRENCE RADIATION LABORATORY
UNIVERSITY of CALIFORNIA BERKELEY

UCRL-17672
ey. 2

DISCLAIMER

Submitted to Nuclear Instruments and Methods

UCRL-17672
Preprint

UNIVERSITY OF CALIFORNIA

Lawrence Radiation Laboratory
Berkeley, California

AEC Contract No. W-7405-eng-48

PHOTOPEAK METHOD FOR THE COMPUTER ANALYSIS OF GAMMA-RAY SPECTRA FROM SEMICONDUCTOR DETECTORS

Jorma T. Routti and Stanley G. Prussin

December 1, 1968

PHOTOPEAK METHOD FOR THE COMPUTER ANALYSIS OF GAMMA-RAY SPECTRA FROM SEMICONDUCTOR DETECTORS

Jorma T. Routti

Lawrence Radiation Laboratory
University of California
Berkeley, California

Stanley G. Prussin

Nuclear Engineering Department
University of California
Berkeley, California

December 1, 1968

Abstract

A method is presented for computer analysis of γ-ray spectra from semiconductor detector systems. We describe a mathematical formalism for the representation of photopeaks and the continua in their vicinity which is applicable to analysis of spectra measured under widely varying conditions. With this formalism the line shape is defined for each peak in the spectrum. The region of data about a single peak or multiple peaks is then fitted with the shape functions and a function representing the background continuum. The line-shape calculations and the fitting are performed by using a least-squares procedure with an iterative gradient minimization method with variable metric. For an automatic analysis an algorithm is developed to search the raw data for statistically significant peaks.

The method has been incorporated into a general-purpose Fortran computer program. In addition to searching and fitting single and multiple peaks, the code performs the energy, efficiency, and line-shape calibrations and makes complete statistical and calibration-error estimates. For establishing the goodness of fit for each peak the output also includes numerical and graphical representation of the fit. Optionally, an on-line cathode-ray-tube display system may be used to assure the completeness of the results even with very complex spectra.

The code has been used with a variety of spectra from Ge(Li) detectors of varying resolution and active volume. The performance is evaluated with test cases and by comparing the results of complete computer and careful hand analysis of ^{177m}Lu and ^{72}As spectra. Applications to spectroscopic measurements and routine data analysis are discussed.

1. Introduction

With the advent of large-volume high-resolution semiconductor diodes and the increasing usage of multichannel analyzers with large memory capacities, the volume and the quality of gamma spectral data have increased enormously. Although these data may be graphically analyzed with good results, the need for a numerical analysis procedure is clearly in evidence. Such a technique would not only provide considerable savings in time but could also lead to significant improvement in the accuracy of data reduction.

The design of a method for numerical data analysis is strongly dependent on the parameters that define the experimental data. Although these may vary considerably with the type of experiment, it is possible to list some requirements that are of general concern:

a. The method should be programmed to perform an automatic data analysis.

b. The method should be capable of handling data measured under a wide variety of experimental conditions, including variable statistics, variable system gains, and detectors of different sizes and quality.

c. The method should be capable of analysis of spectra of high complexity, and no prior knowledge of spectral components should be required. Provisions should be included for the recognition and analysis of closely spaced spectral lines (multiplets).

d. The calibration data, if required, should be readily available.

e. The results of analysis should include γ-ray energies and intensities and the lifetimes of measured lines.

f. The analysis should include calibration procedures for determining energy and efficiency.

g. The accuracy of the results should be as good as the statistics of the data and the accuracy of the calibration information permit. An estimate of the goodness of results and probable errors should be included.

h. The computation procedures should be efficient enough to make the method feasible for routine analysis using available computer capacities.

Several methods have been reported for the computer analysis of sodium iodide scintillation spectra.[1] In most of these the analysis is performed with calculated or measured response functions corresponding to monoenergetic photons, individual isotopes, or other more complex components of the sample. Such response functions are not readily available for semiconductor detectors, and it would be difficult to interpolate such functions to correspond to responses from detectors of different sizes and characteristics. In addition the mathematical problems associated with the response matrix and stripping methods quickly become considerable when the number of peaks and channels in a spectrum becomes large.

The high resolution of the semiconductor detector systems suggests another approach to the analysis of γ-ray spectra. If interest is restricted to the measurements of γ-ray energies and intensities, it is possible to complete an analysis by studying photopeaks only. (The term photopeak is used in the following for both full-energy and escape peaks.) This approach should compare favorably in many respects with the analysis using response functions extending over the whole spectrum. Since no extensive response function information is required, the same techniques can be applied to different detector systems and experimental conditions. Also, since the errors and uncertainties of the analysis

in one part of the spectrum do not propagate into other parts, this procedure is not subject to the accumulation of errors which greatly reduces the accuracy achieved with techniques of spectrum stripping. Although it is true that an analysis restricted to data in the vicinity of photopeaks does not use all the statistical information in the spectrum, the uncertainties caused thereby are probably smaller than the errors introduced by successive stripping of total response functions.

In the following we describe in detail the features of a method for the photopeak analysis of semiconductor γ-ray spectra. The mathematical representation of photopeaks and the techniques for the actual fitting of spectral lines are described in sections 2, 3, and 4. The method developed for search of the spectrum to establish the presence of photopeaks is then described in section 5. These results provide the basis of the computer code, SAMPO, which was written for the analysis of semiconductor spectra (see section 7).

To evaluate the performances of the method and the computer code, calculational techniques were used to analyze data that had previously been subjected to careful graphical analysis. In the following discussions we frequently refer to the analysis of the two complex spectra shown in Figs. 1 and 2. The first of these is a partial γ-ray spectrum of ^{177m}Lu, which was taken with a 1 cm^2 (surface area) $\times$ 5 mm (depletion depth) Ge(Li) detector, and it has the features of excellent statistics and many complex multiplets.[2] The second spectrum, characterized by a large number of photopeaks of widely varying intensities and a wide range of statistics, is from the decay of ^{72}As, and was taken with a Compton shielded detector system with a 7 $cm^2 \times 1$ cm Ge(Li) diode.[3]

2. Functional Representation of Photopeaks and Background Continua

In a simple graphical analysis the continuum under a photopeak can be approximated by a smooth curve through points on both sides of the peak. The area of the peak is then defined as the sum of the counts above the continuum, and the centroid of the peak is taken as the center of gravity. This approach is applicable to only well-defined single lines, and no statistical information in the peak itself is used to define the continuum. Another approach, which can be extended to overlapping peaks, is to fit the data in the vicinity of the peaks with variable-width Gaussian functions and a polynomial or exponential approximation for the background. This approach was tested and found to have serious limitations. With intense photopeaks and good statistics, we often observed significant deviations from a Gaussian shape, particularly on the low-energy side of the photopeaks. Although the width of the Gaussian function should vary smoothly with energy, we found the width to have significant random fluctuations in the regions of less intense peaks of poorer statistics. These deviations introduce considerable errors in resolving multiplets of different intensity ratios, and impose a severe restriction on the ability to analyze overlapping photopeaks.

When determining the locations and areas of photopeaks it would be advantageous to know the correct line shapes and use these representations in the analysis procedure. Such a method would stabilize the analysis procedure and make it possible to use correct shapes for small and overlapping peaks. It would also reduce the number of parameters to be determined for each peak and make the analysis much faster.

The physical and statistical phenomena determining the response of a semiconductor detector to a monoenergetic γ-ray source are quite complex, and the accurate fundamental calculation of peak shapes for the purposes of spectrum analysis is then quite difficult. For this reason and because the peak shapes can be sensitive to small variations in experimental parameters, it is desirable to determine a mathematical representation directly from the measured data. To define a suitable functional representation of the peak shapes it is important to examine some of the factors that determine the line shape. Factors affecting the performance of a Ge(Li) detector system are discussed in the review article by Camp.[4]

The primary factor determining the width of a photopeak is the statistical fluctuation in the division of the absorbed energy between ionization and heating of the crystal lattice. This gives rise to a Gaussian distribution with a small specified width. The extent to which this distribution is reflected in experimental data taken with a particular system is dependent upon a number of factors, the most important being the inherent quality of the detector. The material properties and the impurities in the detector affect the charge collection and the electronic noise associated with leakage current. The combined effects of incomplete compensation of impurities and incomplete charge collection worsen the resolution and give rise to low-energy tailing of the photopeaks. At low energies, the contribution to the resolution from preamplifier noise is important, and, at higher energies, the instabilities of the amplifier and the pulse-height analyzer begin to affect the line width, especially when long counting times are involved. Although the

use of a digital gain stabilizer can decrease this broadening, the stabilization may itself change the shapes of individual lines. Finally, random summing of pulses at high counting rates broadens the peaks and gives rise to tailing. On the basis of these considerations, it is apparent that a mathematical representation of photopeaks should include a basic Gaussian shape whose width is larger than the theoretical resolution of the detector. It should also include provisions for the main deviation from the Gaussian form--that is, the tailing--which can be considerable on the low-energy side of the peaks. In addition to the requirements set by the experimental data, an efficient and stable computational procedure requires the further restrictions that the line shape be described by analytic functions and that the parameters defining the fit be uniquely related to the line shape.

The continuum under the peaks is due to Compton distributions from higher-energy γ-rays and general counting background. Without detailed knowledge of the composition of the spectrum we can say only that the continuum in the short interval under one peak or a cluster of peaks is, except for statistical fluctuations, a continuous, smoothly varying function of energy. Such a function can be approximated with a polynomial.

To test various functional forms, intense, well-isolated photopeaks were analyzed. Several functional forms were tested, and the requirements were best met by the following representation. The central part of a peak is described by a Gaussian and the tails by simple exponentials which join the Gaussian so that the function and its first derivative are continuous. In this representation the shape of a peak is

defined by three parameters: the width of the Gaussian and the distances from the centroid to the junction points. The basic Gaussian form is preserved and included as a special case; fairly severe tailing can be accounted for, and the parameters and the shape are uniquely related. Figure 3 shows a family of these functions on a constant continuum. The width has been kept constant and only the tailing parameter is varied; the same curves are drawn on both linear and logarithmic scales.

3. Shape Calibration Lines

The Gaussian-plus-exponential representation of the shape function for photopeaks has the characteristic that the defining shape parameters vary smoothly with energy and therefore the values of these parameters for any line in a spectrum may be found by interpolation between parameters of neighboring lines. For this purpose, intense and well-isolated lines are used as internal calibrations, and their shape parameters are defined by fitting with the function described and a straight-line approximation for the background continua. This is performed by minimizing the weighted sum of the squares,

$$\chi^2 = \sum_{i=k-\ell}^{k+m} \frac{(n_i - f_i)^2}{n_i} \qquad (1)$$

where i = channel number,

n_i = counts in channel i,

k = approximate center channel of the peak,

ℓ, m = channels specifying the fitting interval,

$$f_i = p_1 + p_2(i-p_4) + p_3 \exp\left[-\frac{(i-p_4)^2}{2p_5^2}\right], \text{for } p_4 - p_6^2 \leq i \leq p_4 + p_7^2,$$

$$f_i = p_1 + p_2(i-p_4) + p_3 \exp\left[\frac{p_6^2\left(2i-2p_4+p_6^2\right)}{2p_5^2}\right], \text{ for } i < p_4 - p_6^2,$$

$$f_i = p_1 + p_2(i-p_4) + p_3 \exp\left[\frac{p_7^2\left(2p_4-2i+p_7^2\right)}{2p_5^2}\right], \text{ for } i > p_4 + p_7^2 .$$

The minimization is performed with respect to the parameters p_j, $j = 1 - 7$ which have the following interpretations:

p_1 = constant in the continuum approximation,

p_2 = slope in the continuum approximation,

p_3 = height of the Gaussian,

p_4 = centroid of the Gaussian,

p_5 = width of the Gaussian (FWHM = 2.355 p_5),

p_6^2 = distance in channels to lower junction point,

p_7^2 = distance in channels to higher junction point.

The straight-line approximation for the continuum under the peak is chosen to stabilize the solution of tailing parameters, and for the same reason these parameters are forced to be positive by being squared.

Once the shape-calibration fit is performed, the best values of the shape parameters p_4, p_5, p_6^2, and p_7^2 are stored from each shape-calibration peak. The line shape in any part of the spectrum is then defined by interpolating the shape parameters linearly with respect to the channel location. The number of calibration fits required depends upon the total energy range of the spectrum. If enough strong, single lines are available we generally use one for about each interval of

100 to 200 KeV in the spectrum. The shape parameters need to be calculated only once for each experimental setup.

The shape calibration is incorporated into program SAMPO. The minimization of the sum in Eq. (1) is performed by subprogram VARMIT, which is an iterative gradient algorithm with variable metric.[5] This routine uses χ^2, its gradient in the parameter space, and the inverse of its second-derivative matrix. The first two quantities are calculated for each iteration step and the third is constructed during the minimization by the method of successive approximations. All this information is used to predict the size and direction of the next iteration step. In addition to the best values for χ^2 and the parameters, the results include a good approximation to the complete error matrix for calculating errors in different parameters. The minimization is terminated when all the components of the next step are less than 10^{-8}, if four succeeding values of χ^2 are the same, or if 100 iterations have been completed. A typical calibration fit is shown in Fig. 4.

The above procedure was used to obtain the shape parameters for calibration lines in the spectra of ^{177m}Lu and ^{72}As. The calibration peaks and shape parameters obtained with these spectra are listed in Table 1. It should be noted that whenever the tailing parameter becomes large compared with the width parameter, its effect becomes negligible and its value need not be accurate.

4. Fitting Single and Multiple Peaks

The primary results of the analysis of γ-ray spectra are the energies and intensities of the photopeaks and the estimated accuracy of these results. The energies are related to channel locations through energy calibration, and the intensities to peak areas through efficiency calibration. The expected accuracy of these values is determined by the statistics of the data and the uncertainties in the calibration procedures. In this section we discuss determination of the channel locations and of the areas of photopeaks, and the associated statistical errors. For each fit a region in the spectrum must be specified. This can be done either by the user or by an automatic algorithm discussed in section 5. The procedures used in the fitting and described below are identical in both cases.

Once the number of lines and the corresponding region of data have been specified for a fit, then the analysis of this region of the spectrum is performed by fitting, in the least-squares sense, the original data points with the line shapes and a polynomial approximation for the continuum. The program SAMPO minimizes the weighted sum of squares

$$\chi^2 = \sum_{i=k-\ell}^{k+m} \frac{\left(n_i - b_i - \sum_{j=1}^{np} f_{ij}\right)^2}{n_i} \qquad (2)$$

where i = channel number,

n_i = counts in channel i,

k = reference channel for background polynomial,

ℓ, m specify the fitting interval,

$b_i = p_1 + p_2(i-k) + p_3(i-k)^2$, background function,

np = number of peaks in the fitting interval,

$$f_{ij} = p_{2+2j} \exp\left[-\frac{(i-p_{3+2j})^2}{2w_j^2}\right], \text{ for } p_{3+2j} - \ell_j \leq i \leq p_{3+2} + h_j,$$

$$f_{ij} = p_{2+2j} \exp\left[\frac{\ell_j(2i-2p_{3+2j}+\ell_j)}{2w_j^2}\right], \text{ for } i < p_{3+2j} - \ell_j,$$

$$f_{ij} = p_{2+2j} \exp\left[\frac{h_j(2p_{3+2j}-2i+h_j)}{2w_j^2}\right], \text{ for } i > p_{3+2j} + h_j.$$

Here parameters p_1, p_2, and p_3 define the continuum, p_{2+2j} and p_{3+2j} are the height and the centroid of j^{th} peak, and w_j, ℓ_j, and h_j are the parameters defining the line shape obtained by interpolating linearly the results of the shape analysis of the calibration peaks.

The minimization is again performed by the VARMIT routine. The initial guess required by this algorithm is obtained from a fast, linear least-squares routine which fits the data with the background approximation plus the correct shape functions, corresponding to the approximate channel locations specified by the user or the search algorithm. The convergence criteria are the same as in the shape analysis.

This computation yields the best values of χ^2 and the parameters, the partial derivatives of χ^2 with respect to parameters calculated, and the error matrix. The channel locations are directly expressed by

the best values of p_{3+2j} and the peak areas are obtained by integrating the shape functions. The final fit is also displayed as a graphical printer plot, showing the original spectral points, the continuum, the sum of the continuum and the shape functions, and the residuals in units of standard deviations of the data points. The optional on-line cathode-ray tube shows also each line in the multiplets. This numerical and graphical information makes it convenient to establish the goodness of the fit and the presence of previously unobserved photopeaks. Figure 5 shows a fitted multiplet in the ^{177m}Lu spectrum as seen on the CRT display.

From the final value of χ^2 and the error matrix we also get estimates for the uncertainties of the parameters computed. Here we have used the standard formulation of least-squares analysis of multivariable functional relationships.[6] Complete analysis of statistical errors in the nonlinear fitting using only approximately correct functional representation would be quite difficult to include in a routine analysis. The linearized error calculation has only limited validity, in that it does not include inaccuracies in the shape functions or the background approximation used. On the other hand the uncertainties in the calibration procedures often dominate the total inaccuracies of the results.

Specifically, the standard deviation of the channel location of the jth peak, p_{3+2j} is expressed as

$$\sigma_{3+2j} = (\chi^2 d_{3+2j,\,3+2j}/nf)^{1/2}, \qquad (3)$$

where nf is the number of degrees of freedom in the fit and $d_{3+2j,\,3+2j}$ is the corresponding diagonal element of the error matrix. The standard deviation of the peak height, $(\chi^2 d_{2+2j,\,2+2j}/nf)^{1/2}$ expressed in per cent of the peak height, is taken to be the uncertainty in the peak area.

To evaluate the accuracy obtained in the fitting procedure a number of test peaks were analyzed. These peaks were generated from measured γ-ray spectra of a ^{203}Hg calibration source counted for different lengths of time with a 1 $cm^2 \times 9$ mm Ge(Li) detector.

Single Peaks on Compton Continuum

Using the measured spectral information, we generated test cases for analyzing single peaks of varying intensities on a Compton plateau and Compton edge of average 2000 counts-per channel. The results are summarized in Table 2. For the peak on the Compton plateau errors found are less than 2% down to a peak-height-to-continuum ratio of 0.3. For the peak on the Compton edge the errors are larger, but less than 5% errors are obtained for ratios of peak height to continuum greater than 1. The error estimates indicated in Table 2 correctly reflect the deviations of the calculated intensity from the known value for the photopeak on the Compton continuum.

Doublets of Various Separations and Intensity Ratios

In all cases the continuum is of a constant intensity (about 1800 counts per channel), as is the higher-energy component for which the peak-height-to-continuum ratio is 1.6. The test cases include three separations between the peaks in the doublet--2.4, 1.2, and 0.6 FWHM--and for each separation ten intensity ratios, 0.025, 0.05, 0.1, 0.25, 0.5, 1.0, 2.5, 5.0, 10, and 40. Figure 6 shows the resulting fit for a doublet of 0.6 FWHM separation and intensity ratio 2.5; this kind of case clearly could not be resolved without the use of shape functions in the fit. The results of all cases considered are summarized in Table 3. In all doublets the components were resolved, and less than 5% errors were encountered

in half of the cases. In the others observed overestimate in the intensity of lower-energy member of the doublet can be explained by the difficulty in fitting the step in the continuum at the location of the stronger peak. The Compton continuum of the peak itself introduces a discontinuity in the background which affects the results significantly only if a small peak lies very close to a strong line. This difficulty could be lessened by an additional parameter in the peak shape function or by an additional degree of freedom in the background approximation. These generalizations would, however, require improved data for the shape calibration and add to the complexity of the analysis. Especially with complex spectra with high continua these disadvantages outweigh any improvement in the accuracy, and consequently have not been incorporated in the general-purpose code.

5. Automatic Peak Search and Selection of Fitting Intervals

To perform an automatic analysis of γ-ray spectra we need to provide the program with an algorithm that will locate the peaks initially and choose the intervals for fitting.

If the data could be obtained as a smooth, continuous curve, then a peak could be easily recognized as a sharp local maximum. Further, the second derivative or the curvature of the plotted data would have a fairly small value except in the vicinity of a peak. The data obtained with multichannel analyzer, however, have more or less severe fluctuations throughout the entire spectrum because of the discrete and statistical nature of the data. The search routine must therefore apply some statistical criteria to test the presence of real peaks. Because a peak is ordinarily several channels wide, one can use some smoothing

procedure to damp the inherent local fluctuation without losing much of the features characterizing the peaks. Recently Inouge and Rasmussen[7] discussed a peak-search routine which uses a smooth curve obtained through Fourier transformation, and Mariscotti[8] has discussed an approach that uses generalized second-difference operations. The search algorithm which we have included in the code uses some of the techniques proposed by Mariscotti, and is discussed in the following.

A simple numerical second difference dd_i in channel i is expressed as

$$dd_i = -n_{i-1} + 2n_i - n_{i+1} = \sum_{j=-1}^{+1} c_j^0 n_{i+j} \tag{5}$$

Because of the local fluctuations this expression as such is not applicable to peak search. It can be generalized by defining (2k + 1) multipliers c_j in the expression

$$dd_i = \sum_{j=-k}^{+k} c_j n_{i+j} \tag{6}$$

With the proper choice, the coefficients c_j, together with the standard deviation,

$$sd_i = \left[\sum_{j=-k}^{+k} c_j^2 n_{i+j} \right]^{1/2} \tag{7}$$

can be used to recognize peaks in the spectrum by computing the significance of the second difference $ss_i = dd_i/sd_i$ and comparing it with a given threshold value. The coefficient c_j should be chosen to optimize

this procedure--that is, to detect as small a significant peak as possible on a constant background. This optimization can be simplified if a procedure is chosen to get c_j's, and the parameters governing this procedure are optimized. Using integration rather than summation notation, we can write

$$dd(x_0) = \int_{-\infty}^{\infty} c(p, x)n(x-x_0)dx \tag{8}$$

$$sd(x_0) = \left\{ \int_{-\infty}^{\infty} \left[c(p, x) \right]^2 n(x-x_0)dx \right\}^{1/2} \tag{9}$$

and optimize $c(p, x)$ with respect to parameters p. We propose that $c(p, x)$ be chosen to be the second derivative of a Gaussian,

$$c(p, x) = - \frac{d^2}{dx^2} \left[\exp\left(- \frac{x^2}{2p^2} \right) \right] = \frac{p^2 - x^2}{p^4} \exp\left(- \frac{x^2}{2p^2} \right) \tag{10}$$

Assuming that

$$n(x-x_0) = a \exp\left[- \frac{(x-x_0)^2}{2\sigma^2} \right] + b \tag{11}$$

and letting $z = p/\sigma$, we will have

$$dd(x_0) = \frac{a(2\pi)^{1/2}}{\sigma z} \left[\frac{1}{(1+z^2)^{1/2}} - \frac{1}{(1+z^2)^{3/2}} \right] \tag{12}$$

$$\left[sd(x_0) \right]^2 = \frac{a(2\pi)^{1/2}}{\sigma^3 z^3} \left[\frac{1}{(2+z^2)^{1/2}} - \frac{2}{(2+z^2)^{3/2}} + \frac{3}{(2+z^2)^{5/2}} \right] + \frac{3b(\pi)^{1/2}}{4\sigma^3 z^3} \tag{13}$$

The optimization can be defined as the maximation of dd/sd for a given a and b, that is,

$$\frac{d}{dz}\left[\frac{dd}{sd}\right]_{x_0} = 0 . \tag{15}$$

The resulting optimal z as a function of b/a is shown in Fig. 7. The significance of a peak is measured by ss = dd/sd. To compute the minimum amplitude of a detectable peak we equate dd/sd with a threshold value t. The computation of the resulting minimum amplitude, using the asymptotic value z = 2.3 from Fig. 7, yields

$$a_{min} = \frac{0.23\ t^2}{\sigma} + \left[\frac{0.053\ t^4}{\sigma^2} + \frac{0.85\ t^2 b}{\sigma}\right]^{1/2} \tag{16}$$

For $b >> 0$ -- that is, for a peak on a high background -- we get

$$a_{min} \simeq 0.92\ t \left(\frac{b}{\sigma}\right)^{1/2} \tag{17}$$

When applying the search algorithm to a complex spectrum it is generally more difficult to detect all the components of multiplets than to detect small peaks in a constant background. To enhance the detection of the small components we can make the weighting function c(p, x) narrower, that is, choose a smaller value for z. As pointed out by Mariscotti, the optimal choice of z for multiple peaks depends upon the separation and the background ratios of the components; no one value is optimal in a general case. We have chosen to use $p = \sigma$ -- that is, z = 1 -- in the weighting function. The reduction in the sensitivity in the detection of a single peak is not serious, and the minimum detectable amplitude in this case is for $b >> 0$,

$$a_{min} \simeq 1.33\, t \left(\frac{b}{\sigma}\right)^{1/2} \tag{18}$$

In a search algorithm applied to discrete data measured with a multichannel analyzer, we use, rather than integration, summation over a set of weighting coefficients c_j. The coefficients c_j are defined as

$$c_j = \frac{p^2 - j^2}{p^4} \exp\left(-\frac{j^2}{2p^2}\right), \quad j = 0, \pm 1, \pm 2, \ldots, \pm k \tag{19}$$

where p is $\sigma_{av} = FWHM_{av}/2.355$ of the peaks in the spectra. The set is terminated at k, where $c_{k+1} < 0.01\, c_0$. The second coefficient is then adjusted so that the sum of coefficients is zero. The resulting coefficients for certain values of σ are listed in Table 4. These are quite similar to those obtained by Mariscotti by a double-averaging procedure starting from the simple second-difference coefficients (-1, 2, -1). In Mariscotti's procedure the generalized second difference is defined as

$$dd_i(p_1, p_2) = \underbrace{\sum_{j=i-p_2}^{i+p_2} \cdots \sum_{k=\ell-p_2}^{\ell+p_2}}_{p_1} dd_k \,, \tag{20}$$

where

$$dd_k = n_{k-1} + 2n_k - n_{k+1} \,.$$

The optimal values of parameters p_1 and p_2 were found to be $p_1 = 5$ and $p_2 = 0.3\ FWHM - 0.5$. The last row in Table 4 gives these coefficients c_j for $\sigma = 3\text{-}4$, normalized to $c_0 = 100$.

In addition to the computed statistical significance of a potential peak, additional tests derived from the shape of a peak can be used. Of the tests proposed by Mariscotti we have incorporated one in the algorithm. The number of channels whose second-difference expression has the same sign as the peak channel is compared with a number predicted on the basis of the Gaussian shape of the peak. The number of channels x_1 from the peak centroid to the point at which the sign of the second difference changes can be determined from the equation

$$\int_{-\infty}^{\infty} \frac{p^2-(x-x_1)^2}{p^4} \exp\left[-\frac{(x-x_1)^2}{2p^2}\right]\left[a \exp\left(\frac{-x^2}{2\sigma^2}\right)+b\right] dx = 0 \qquad (21)$$

For $p = \sigma$ the solution is $x_1 = 2(\sigma)^{1/2}$ and the expected number of channels in the region of the unchanged sign is $2x_1$. An acceptable tolerance of ± 2 or $0.5x_1$, whichever is larger, is used in connection with this test.

A search algorithm based on the method described above has been incorporated into program SAMPO. The coefficients for the generalized second difference are first computed by using information on the peak width from the shape-calibration results. The statistical significance of the second difference is then computed for each channel and it is compared with two threshold values. The lower defines potential peaks and the higher defines the acceptance level; these values are normally 2 and 5, respectively. The accepted peaks have also to pass the peak-shape test described above in order to enter the array of peaks to be fitted.

The use of the algorithm has been found quite satisfactory for routine analysis. The computing time on the CDC-6600 machine is only

about 2 seconds per 1600-channel spectrum. We have found it preferable, in careful spectroscopic analysis, to have options to add or drop peaks in the list before the fitting procedure. This can be done by using the on-line cathode-ray-tube display system or by performing the analysis in two runs. The first run produces a plot of the spectrum and a list of peaks found. The list can be corrected in the second run on the basis of careful visual inspection of the data, and thus the completeness of the list is improved before more time-consuming fitting is done. As pointed out earlier, some small components in multiplets can be detected only in the fitting procedure. In the analysis of the ^{177m}Lu spectrum all but the weak 182.0-keV line and the small components in doublets at 117.2, 145.8, 262.9, 283.4, 292.5, and 433.7 keV were detected.

Another part of the automated analysis is the selection of fitting intervals and number of peaks included in each fit. A requirement for fitting a single peak is that the peak be sufficiently isolated from neighboring photopeaks so that the interference from these is negligible; this requirement is fulfilled in most cases. However, in order to resolve overlapping peaks or to make determination of the background for closely spaced peaks more accurate, it is necessary to fit them simultaneously. In selection of fitting intervals peaks represented by less than a given separation parameter, generally six times FWHM, are fitted together.

A preliminary choice of the total region included in the fit is made by locating local minima in the spectrum averaged over five channels; up to three times FWHM are included on either side of the peak. With large statistical fluctuations it is advantageous to include more channels in the interval to define the continuum more accurately. For this purpose

an effort is made to extend the interval obtained above by drawing a straight line through the two minima found and studying the deviations of additional points in the spectrum from this line. If these are less than a prescribed deviation--say three standard deviations the number of counts in that channel--the interval is extended to include this channel. Up to another two times FWHM may be included in this way. If the final interval remains smaller than a specified lower limit, typically six times FWHM, then no parabolic correction is applied for the continuum; this is done to avoid grossly erroneous background approximations when not enough information is available for the determination of the parabolic correction.

6. Analysis of Test Spectra

The performance of the method and the computer program were evaluated by analysis of ^{177m}Lu and ^{72}As spectra. The following discussion is confined to the essential fitting results, that is, determination of exact channel locations, and more specifically the photopeak areas. With both spectra, computer results are compared with the results from very carefully performed independent graphical analysis.[2,3]

^{177m}Lu Spectrum

The results from the shape analysis and the search routine have already been discussed above. Comparison between computer and graphical analysis is summarized in Table 5. Agreement between the two sets of results is quite satisfactory in all photopeak intensity groups, especially when the discrepancies are compared with the uncertainties in the energy and efficiency calibrations, typically 0.1 keV and 5%

respectively. When studying the individual peaks we notice that the most severe discrepancies occur in a few multiplets. We have summarized these cases in Table 6 , where the two results are compared with results from a more recent measurement using a higher-resolution detector. It is evident from these examples that the results of the computer analysis more accurately describe the intensity ratios in these multiplets. One of the multiplets referred to is shown in Figs. 8, 9, and 10. Figure 8 displays the fit to the three peaks found by the search routine. The unobserved peak is clearly revealed by the correct line-shape functions and also by the residuals in the fit. Figure 9 shows the same data with four lines. A relative intensity 0.80 was assigned to 292.5- and 291.4-keV lines, rather than 1.00, as obtained in the graphical analysis. Figure 10 shows the same region in the higher-resolution spectrum, which yielded a relative intensity of 0.79 for these lines.

^{72}As Spectrum

A comparative study of the results obtained in the graphical and the computer analyses has also been performed with the spectrum of ^{72}As shown in Fig. 2. In general the discrepancies between the two results are somewhat larger than those in the ^{177m}Lu spectrum. This is mainly due to the less favorable conversion gain used and much weaker statistics at the high-energy end of the spectrum. Table 7 summarizes the results in different intensity groups; again the agreement can be considered very satisfactory.

7. Energy and Efficiency Calibrations

The high resolution of the Ge(Li) systems and the accurate procedures for determination of the centroids and the areas of the photopeaks set stringent requirements for the calibration techniques. Within the computer code we also want a high degree of flexibility in the calibration procedures, for instance, in order to use some fitting results as calibrations for the others.

Energy Calibrations

Deviations from the basically linear energy response of the preamplifier and the analog-to-digital converter of the multichannel analyzer give rise to integral nonlinearities. These may add up to few parts in a thousand, and must be accounted for in an accurate energy calibration. The nonlinearity may have any form; however, it may be assumed to be a continuous function of energy.

We have incorporated into the analysis two methods for energy calibration. The first routine uses any number of energy-calibration points and interpolates linearly between these points. In the second method a polynomial least-squares fit is made to these points and the resulting curve is used for energy calculation. In both approaches an estimate of the errors associated with the energy calibration is also needed. These uncertainties reflect the inaccuracies in the energies and channel locations of the energy-calibration peaks, expected drifts in the detector system, and errors in the energy determination itself. These uncertainties are expressed as a band around the energy calibration curve; the width of which is specified at different energies and interpolated linearly between them.

Figure 11 summarizes the energy calibration results obtained in a system of very good linearity.[9] The graph shows the integral nonlinearity of the response and the corresponding polynomial fit of fifth order. The linear interpolation and the polynomial expansion give consistent results, and either one may be used. Figure 12 shows a more significant nonlinearity of a system employing a biased amplifier. Here strong lines of a complex spectrum of ^{176}Ta have been used as internal energy standards.[10] In this case a polynomial of a high order is required to obtain a good fit; however, this introduces nonrealistic oscillations between the calibration points. That the polynomial expansion should not be used beyond the extreme data-calibration points is well exemplified by this case.

The energies of the photopeaks are assigned by using either one of the two procedures. The uncertainty in the energy is obtained by adding in root-mean-square sense the calibration error at that energy and the statistical uncertainty in the peak centroid translated into the energy units. In most cases the calibration errors dominate the total uncertainties, and depending on how stable the system is and how much effort is spent in the calibration procedures the energies of strong lines may be determined with an accuracy up to 0.02 to 0.2 keV or 0.01%.

Efficiency Calibrations

Some of the factors that determine the counting efficiency are intrinsic full-energy peak efficiency, counting geometry, and self-absorption in the source. Due to the uncertainties in these factors no adequate scheme is presently available for calculation of the efficiency, but rather it must be determined experimentally for each type of detector.

Efficiency-calibration procedures similar to the energy calibrations have been incorporated into the code. The interpolation scheme again is flexible enough to accurately describe any curve when enough points are used. An approximate functional form that assumes basically linear relation between the energy and efficiency on the logarithmic scale may also be used. As with the energy calibration, the overall accuracy obtained depends largely on the stability of the system and on the quality of the calibration data. At best, accuracies approaching the statistical uncertainties--that is, about 1 to 3%--can be obtained with relative intensities of strong lines. The uncertainty in the intensity calculation is again obtained by adding in the root-mean-square sense the calibration and statistical uncertainties.

8. Computer Program SAMPO

The complete analysis described above is performed by a computer program SAMPO,* written in Fortran language. The schematic block diagram of the code is shown in Fig. 13. All calibration procedures required in the analysis are performed within the code; the user needs only to provide the spectral data on cards or magnetic tape. The output contains, in addition to the numerical results, graphical information on each fit in the form of a printer plot and optionally pen-drawn graphs such as shown in this report. A substantial effort has been made to make the code flexible enough to be easily applicable in a wide range of problems ranging from accurate nuclear spectroscopic work to routine data reduction.

*This name has been taken from Finnish mythology (Kalevala epos), in which a miracle mill known as Sampo fulfills all the wishes of its owner.

The code is provided with a large number of internal decision-making algorithms which permit automatic off-line data reduction. However, for the analysis of very complex spectra and also for demonstration purposes, we have included in the code optional interactive input-output facilities employing an on-line cathode-ray-tube display system with teletype and light-pen input. An accurate graph of the spectrum with indications of the peaks found by the search algorithm is first displayed on the screen. The list of peaks found may then be edited by adding peaks to it or dropping them by using the light pen; this is recommended to ensure the completeness of the list before more time-consuming fitting procedure. The editing can also be done in off-line runs, but then two runs are necessary to complete the results; however, only spectra of high complexity normally require any editing. In the on-line analysis the user may next let the code fit all the peaks automatically, inspect the fitting results, and intervene only in case of difficulty. Or he may select the fitting intervals manually. In either case a graph such as shown in this text is displayed for each fit. The calibration results may also be displayed on the screen. In short, the on-line features make it possible to ensure completeness of the results in one run, even with the most complex spectra.

We have run the code on the CDC-6600 machines of Lawrence Radiation Laboratory, Berkeley. The multiprogram features of the operating system easily allow the usage of the on-line procedures without decreasing the computers' efficiency. An experimental version of the code allows two users using two display systems to analyze their spectra independently.[11] Extensive use is here made of the fast disk

storage with roll-in and roll-out operations, which accounts for a significant decrease in computer memory requirements. The execution time of the search algorithm is about 1 second per 1000 channels. The central processor time required in the fitting depends on the complexity of the spectrum and the number of channels in a typical peak, that is, the gain of the system. Normally about 1 second per photopeak is required; for instance, the complete analysis of the ^{177m}Lu and ^{72}As spectra can be performed in off-line batch processing by using about 1 minute of central processor time.

9. Applications of the Analysis Method

The methods described and the computer program SAMPO have been used extensively both in the analysis of nuclear spectroscopy data and in routine data reduction for the past two years. The study of energy levels in ^{72}Ge from the decays of ^{72}Ga and ^{72}As, the latter referred to in the text, was completed with the exclusive use of the computer analysis.[3] Other nuclear spectroscopy applications have relied heavily on the on-line features in the analysis of very complex gamma-ray spectra,[9] including poor-statistics coincidence data.[10]

Although primarily designed for the analysis of semiconductor γ-ray spectra, the method has been found applicable to electron spectra[10] and also to simple γ-ray spectra measured with NaI(Tl) detectors.[12] Preliminary studies have been performed in the use of the code in alpha spectroscopy; here it may be necessary to slightly modify the functional form of the line shape to account for the significant low-energy tailing seen in alpha peaks. As such, or with modified functional representation, the method should be applicable to a wide range of spectroscopy problems in which the measurement can be based on analysis of single and multiple peaks.

ACKNOWLEDGMENTS

The continuous support and cooperation of Alan R. Smith and Roger Wallace is gratefully acknowledged. We thank A. J. Haverfield, Frederick M. Bernthal, Jack M. Hollander, and David Camp for their data and results to be compared as well as for helpful discussions. The data handling effort was helped by the assistance of Nickey F. Little, and programming by consultations with Eric R. Beals, William H. Benson, and William F. Dempster.

The first author is grateful to Professor Pekka Jauho of Helsinki Technical University for continuous encouragement.

References

*Work done under auspices of the U. S. Atomic Energy Commission.

1. Application of Computers to Nuclear and Radiochemistry, NAS-NS-3107, 1962.
2. A. J. Haverfield, F. M. Bernthal, and J. M. Hollander, New Transitions and Precise Energy and Intensity Determination in the Decay of ^{177m}Lu, Nucl. Phys. A94 (1967), 337.
3. David C. Camp, Energy Levels in ^{72}Ge from the decays of ^{72}Ga and ^{72}As, Nucl. Phys. A121 (1968), 561.
4. David C. Camp, Application and Optimization of the Lithium-Drifted Germanium Detector Systems, UCRL-50156, Mar. 1967.
5. W. C. Davidon, Variable Metric Method for Minimization, ANL-5990, 1959; E. Beals, VARMIT, Lawrence Radiation Laboratory memo BKY-ZO (unpublished).
6. Experimental Statistics, Nat. Bur. Std. (U. S.), Handbook 91, 1963.
7. T. Inouge and N. C. Rasmussen, A Computer Method for the Analysis of Complex Gamma-Ray Spectra, in Trans. Am. Nucl. Soc. 1967 Annual Meeting, (American Nuclear Society, Chicago, 1967).
8. M. A. Mariscotti, A Method for Automatic Identification of Peaks in the Presence of Background and Its Application to Spectrum Analysis, Nucl. Instr. Methods 50 (1967) 309.
9. J. B. Wilhelmy, S. G. Thompson, J. O. Rasmussen, and J. T. Routti, Spectroscopic Studies of Short-Lived Fission Products, UCRL-18248 Abs., 1968.

10. F. M. Bernthal, I. The $|\Delta K| = 1$ Electric Dipole Transitions in Odd-Mass Deformed Nuclei. II. The Decay of ^{176}Ta to Levels in ^{176}Hf (Ph. D. thesis), UCRL-18651, in preparation.

11. William Benson, (Lawrence Radiation Laboratory), private communication.

12. J. Miller, J. T. Routti, A. R. Smith, and W. W. Wadman, Neutron Attenuation Studies for Medium-Energy Cyclotron Beams, UCRL-18280, in preparation.

Table 1. Parameters defining peak shapes used in analysis of spectra. All numbers except chisquares in units of channels.

Channel	Width parameter	Std. dev. of width	Low-tail parameter	High-tail parameter	Chi-square	Chi-square Gaussian	Channels in fit
^{177m}Lu Spectrum							
241.8	2.041	0.004	3.80	20.6	122.3	480.4	24
328.1	2.092	0.003	4.09	28.2	93.4	262.0	23
420.5	2.130	0.004	3.83	27.2	103.1	392.4	24
701.6	2.285	0.005	3.89	63.0	195.8	1162.3	27
781.1	2.334	0.009	3.54	33.1	54.7	176.4	35
1074.2	2.493	0.010	3.81	15.3	117.5	632.7	28
1264.7	2.599	0.010	4.01	14.3	122.4	829.4	27
1442.7	2.696	0.060	3.96	7.1	27.2	28.1	29
^{72}As Spectrum							
783.1	1.062	0.017	1.52	1.42	12750	100984	21
986.7	1.121	0.009	1.55	1.45	40.4	355.	24
1306.2	1.264	0.020	1.58	4.83	23.4	49.6	23
1607.6	1.294	0.014	1.85	2.13	11.0	23.7	23
1871.8	1.423	0.017	4.46	2.40	23.1	29.4	22
2465.4	1.575	0.017	2.22	2.73	16.9	40.0	29
3579.1	1.836	0.043	2.02	3.65	26.6	47.8	35

Table 2. Single lines of different intensity on Compton plateau of 1800 counts per channel and on Compton edge of 2100 counts per channel.

Peak height / Compton plateau	Fitted intensity / True intensity	Peak height / Compton edge	Fitted intensity / True intensity
0.035	1.246 ± 0.267	0.03	2.256 ± 0.307
0.07	1.084 ± 0.139	0.06	1.588 ± 0.157
0.14	1.068 ± 0.072	0.12	1.329 ± 0.079
0.35	1.009 ± 0.031	0.3	1.120 ± 0.033
0.7	1.014 ± 0.016	0.6	1.078 ± 0.017
1.4	1.001 ± 0.009	1.2	1.038 ± 0.009
3.5	1.000 ± 0.006	3.0	1.023 ± 0.005
7.0	0.999 ± 0.005	6.0	1.015 ± 0.005
14.	1.007 ± 0.004	12.	1.021 ± 0.005
35.	0.998 ± 0.005	30.	1.011 ± 0.005

Table 3. Analysis of doublets of different separations and intensity ratios on Compton plateau of 1800 counts per channel. The higher channel peak is of constant intensity with a ratio of peak height to Compton plateau of 1.6.

	Fitted intensity ratio/true intensity ratio		
Intensity ratio	Separation (F WHM)		
	2.4	1.2	0.6
0.025	1.702 ± 0.294	1.388 ± 0.382	3.786 ± 2.840
0.05	1.311 ± 0.160	0.919 ± 0.144	2.651 ± 1.378
0.1	1.180 ± 0.084	1.080 ± 0.111	1.910 ± 0.536
0.25	1.048 ± 0.039	1.015 ± 0.044	1.195 ± 0.154
0.5	1.031 ± 0.020	1.026 ± 0.023	1.125 ± 0.071
1.0	1.006 ± 0.018	1.013 ± 0.015	1.046 ± 0.029
2.5	0.995 ± 0.015	1.004 ± 0.015	0.990 ± 0.047
5.0	0.988 ± 0.016	0.994 ± 0.018	0.873 ± 0.069
10.	0.987 ± 0.021	0.989 ± 0.026	0.696 ± 0.113
25.	1.244 ± 0.058	0.948 ± 0.051	0.538 ± 0.310

Table 4. Coefficients for the generalized second difference

$$\text{in } dd_i = \sum_{j=-k}^{k} c_j n_{i+j} .$$

σ = p	2k+1	c_j	j=0, ±1, . . . , ± k						
0.5	3	100.	-50.0						
1.0	7	100.	- 0.5	-40.6	- 8.9				
2.0	15	100.	65.6	0.	-40.6	-40.6	-23.1	- 8.9	- 2.4
3.0	23	100.	83.4	44.8	0.	-32.0	-44.3	-40.6	-29.2
		- 17.5	- 8.9	- 3.9	- 1.5				
4.0	31	100.	90.0	66.2	33.2	0.	-25.8	-40.8	-44.6
		40.6	-32.3	-23.1	-15.0	- 8.9	- 4.9	- 2.5	- 1.1
Coefficients by Mariscotti									
3 to 4	23	100.	90.6	62.5	15.6	-18.8	-40.6	-50.	-76.7
		- 31.3	-18.8	- 9.4	- 3.1				

Table 5. Summary of comparison of computer and graphical (used as standard) analysis of the ^{177m}Lu spectrum.

Integrated number of counts	Peaks in the group	Deviations			
		Mean arith. channel (channels)	Mean absolute channel (channels)	Mean arith. area (%)	Mean absolute area (%)
10^3-10^4	2	-0.15	0.15	+0.7	0.7
10^4-10^5	7	-0.06	0.07	+0.1	1.1
10^5-10^6	15	-0.06	0.08	-1.2	1.5
10^7-10^8	7	-0.08	0.09	+0.5	0.7
All above	31	-0.07	0.08	-0.4	1.2

Table 6. Some multiplets in ^{177m}Lu.

Energy (keV)	Channel				Area				Relative intensity		
	Comp.	Uncert.	Diff.	Graph.	Comp.	Uncert. %	Diff. %	Graph.	Graph.	Comp.	High resolution
145.8	392.39	0.03	0.29	392.1	7.83 E+4	1.0	8.6	7.22 E+4	22.9	26.6	26.5
147.2	397.63	0.01	0.03	397.6	2.95 E+5	0.3	-5.8	3.13 E+5	100.	100.	100.
281.8	901.72	0.01	-0.08	901.8	2.46 E+5	0.3	0.1	2.45 E+5	100.	100.	100.
283.4	909.03	0.10	1.08	907.95	7.68 E+3	4.0	-27.3	1.06 E+4	4.31	3.13	2.80
291.4	938.50	0.07	0.50	938.0	1.71 E+4	3.0	6.1	1.61 E+4	100.	100.	100.
292.5	942.28	0.09	0.18	942.10	1.37 E+4	3.6	-15.2	1.61 E+4	100.	80.1	79.1
313.7	1021.73	0.04	0.33	1021.40	1.68 E+4	1.3	9.9	1.53 E+4	11.5	12.6	12.1
319.0	1041.62	0.01	0.02	1041.60	1.33 E+5	0.4	0.0	1.33 E+5	100.	100.	100.
321.3	1050.23	0.04			1.52 E+4	1.5	-9.1	1.67 E+4	12.6	11.4	10.1

Table 7. Summary of the comparison of the computer and the graphical (used as standard) analyses of the ^{72}As spectrum.

Integrated number of counts	Peaks in group	Percent deviation of peak area	
		Mean arith.	Mean absolute
10^1-10^2	6	-1.33	5.17
10^2-10^3	28	-1.63	5.90
10^3-10^4	25	+2.57	4.27
10^4-10^5	12	-0.7	2.99
All of above	71	+0.07	4.77

FIGURE CAPTIONS

Fig. 1. Partial γ-ray spectrum of ^{177m}Lu counted with a $1\ cm^2 \times 0.5$ cm Ge(Li) detector with FET preamplifier.

Fig. 2. Gamma-ray spectrum of ^{72}As counted with a Compton-shielded system with $7\ cm^2 \times 1\ cm^2$ Ge(Li) diode.

Fig. 3. Line-shape functions with various degrees of tailing. The Gaussian is extended with exponential at C so that the function and the slope are continuous. The same functions are drawn on logarithmic and linear scales. $y = 1 + 10 \exp(-x^2/2)$, for $x \leq c$; $y = 1 + c_1 \exp(-c_2 |x|)$, for $|x| > c$.

Fig. 4. Shape-calibration fit to a photopeak with some tailing on the low-energy side only (upper scale). The residuals are expressed on the lower linear scale in units of standard deviation of the data.

Fig. 5. A multiplet in the ^{177m}Lu spectrum resolved by fitting the data with the energy-dependent shape functions. Residuals (lower scale) are expressed in standard deviations of the counts measured.

Fig. 6. Doublet of FWHM separation 0.6 and intensity ratio 2.5. The calculated ratio is 2.48 ± 0.04.

Fig. 7. Optimal parameter in generalized second-difference expression for different background-to-peak ratios.

Fig. 8. Fit to a multiplet in the ^{177m}Lu spectrum, with indication of a missing component in the lowest-energy peak. Residuals (lower scale) are expressed in standard deviations of the counts measured.

Fig. 9. Complete fit to a multiplet also shown in Fig. 8.

Fig. 10. Fit in the higher-resolution data to the same multiplet as shown in Figs. 8 and 9.

Fig. 11. The energy calibration of a system with small nonlinearity. The calibration points, the interpolation results, and the fifth-order polynomial fit are displayed with assigned uncertainties.

Fig. 12. The energy calibration of a Ge(Li) system with significant nonlinearity. Unrealistic oscillations appear between calibration points, and especially beyond the last calibration points in polynomials of third, fifth, and ninth order.

Fig. 13. Schematic block diagram of the computer program SAMPO.

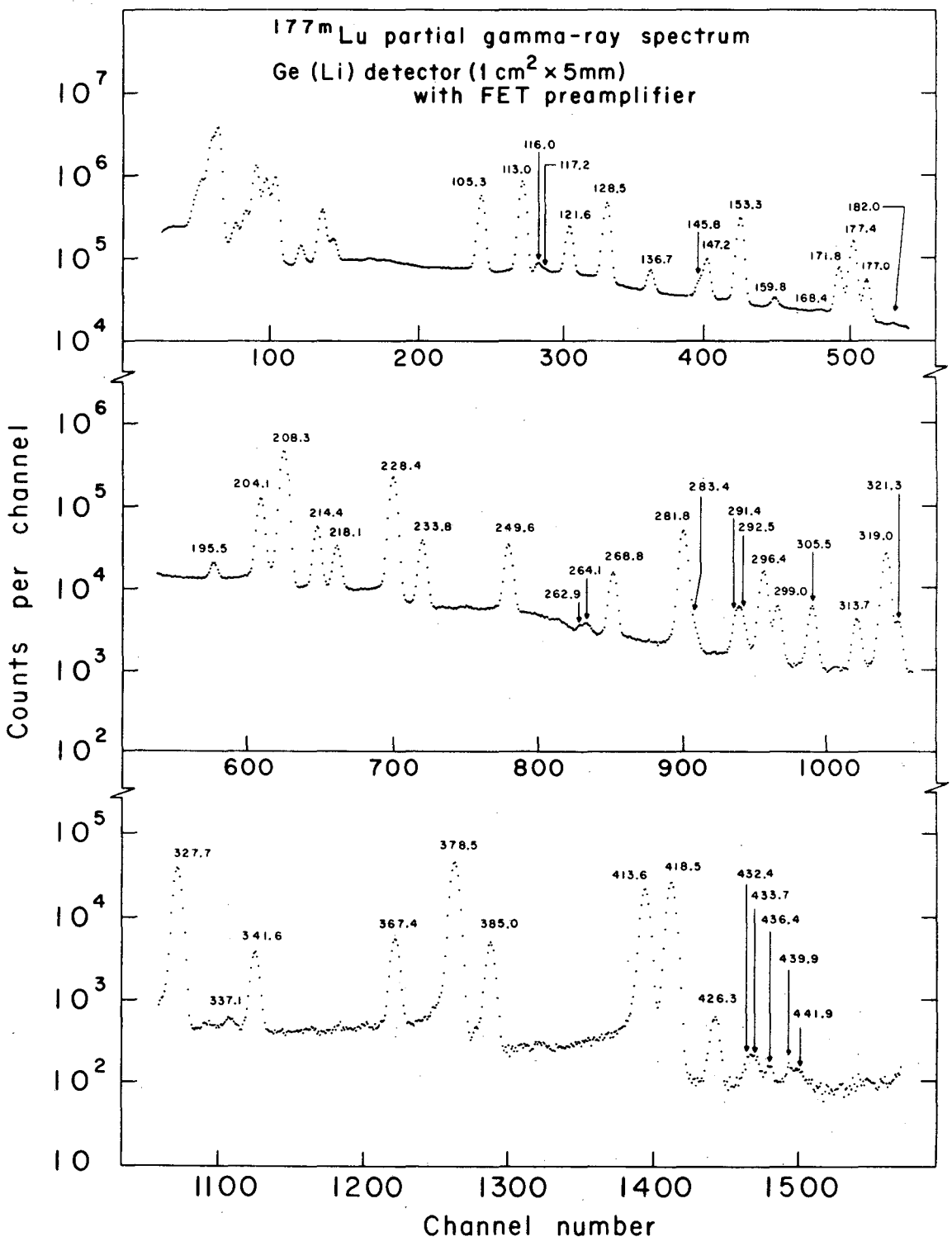
177m Lu partial gamma-ray spectrum
Ge (Li) detector (1 cm² x 5mm)
with FET preamplifier
Counts per channel
Channel number
105.3
113.0
116.0
117.2
121.6
128.5
136.7
145.8
147.2
153.3
159.8
168.4
171.8
177.0
177.4
182.0
195.5
204.1
208.3
214.4
218.1
228.4
233.8
249.6
262.9
264.1
268.8
281.8
283.4
291.4
292.5
296.4
299.0
305.5
313.7
319.0
321.3
327.7
337.1
341.6
367.4
378.5
385.0
413.6
418.5
426.3
432.4
433.7
436.4
439.9
441.9
XBL670-5374

Fig. 1

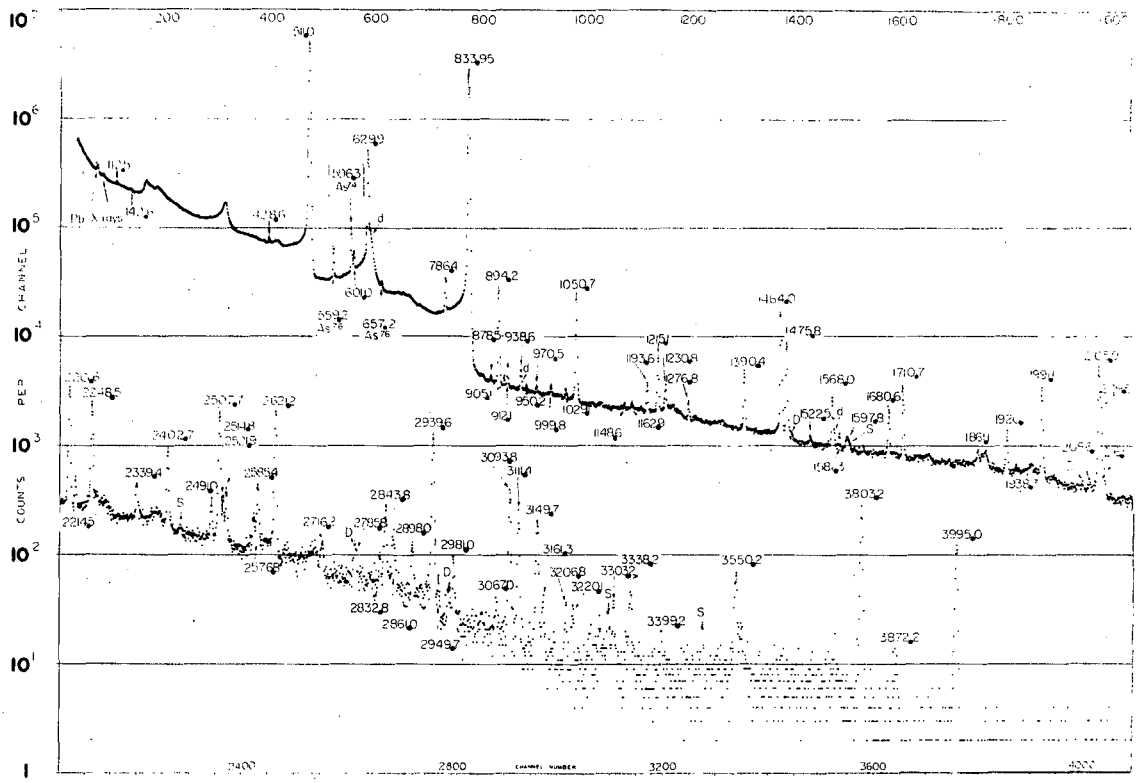

Fig. 2

XBL 691-136

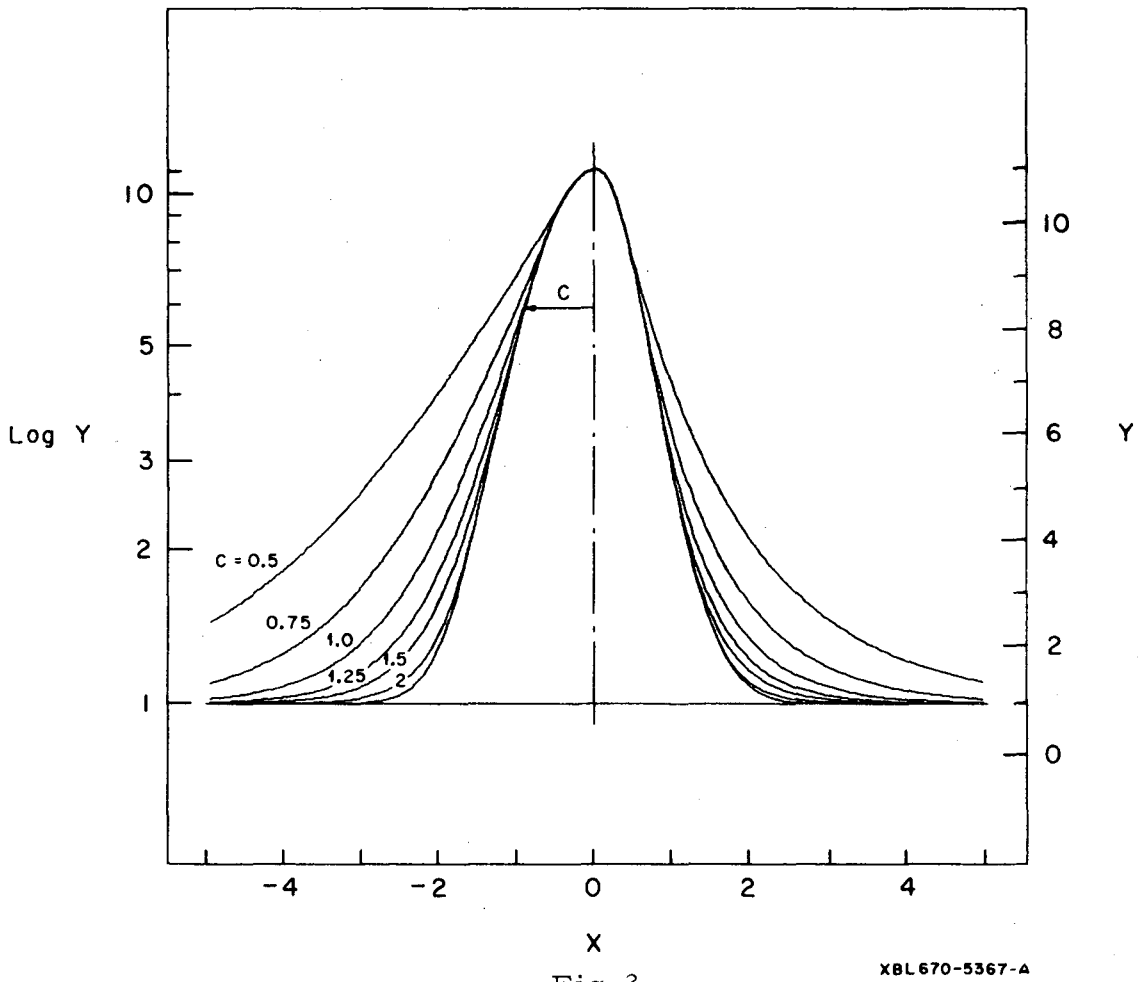
Log Y
10
5
3
2
1
c = 0.5
0.75
1.0
1.25
1.5
2
c
10
8
6
4
2
0
Y
-4
-2
0
2
4
X
XBL670-5367-A

Fig. 3

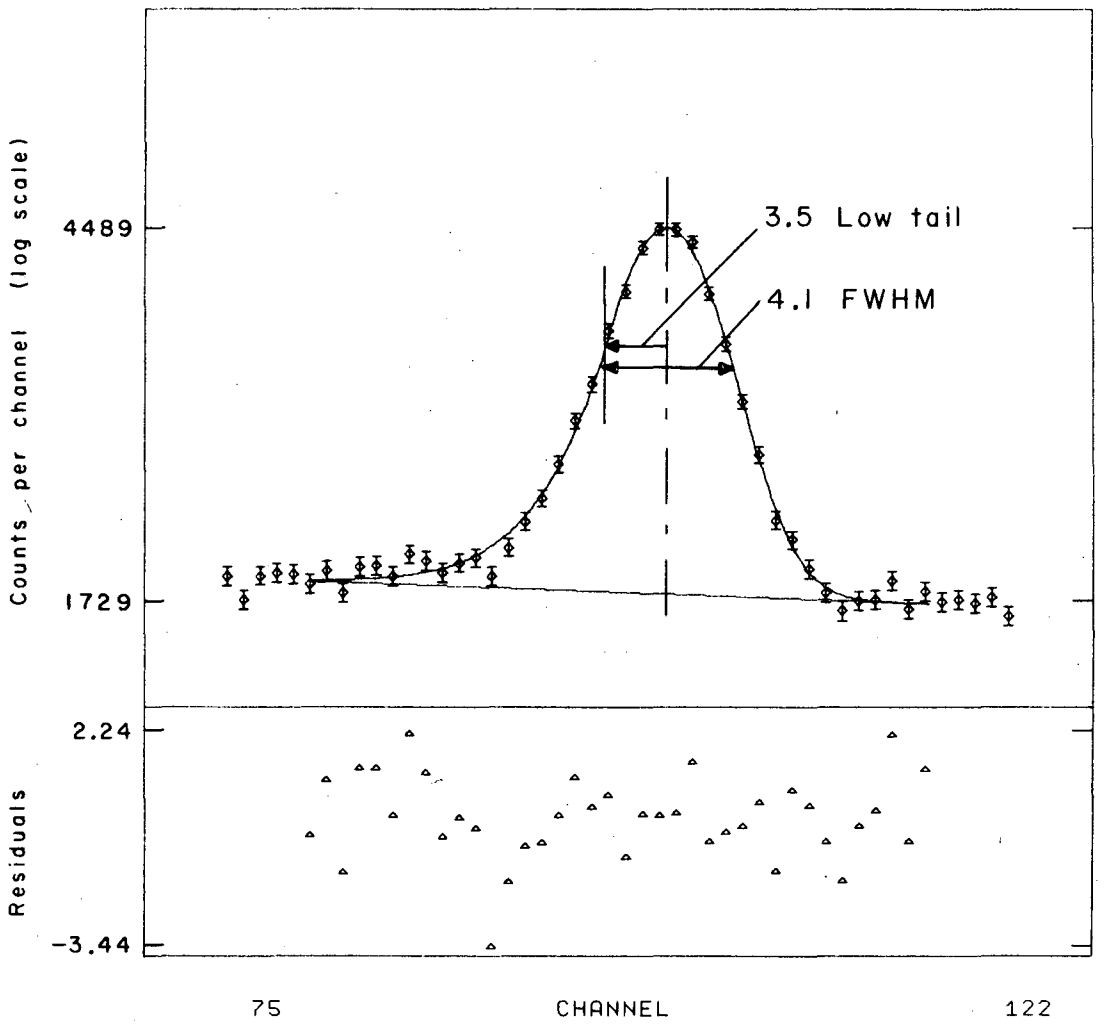

Fig. 4

XBL 6710-2145-A

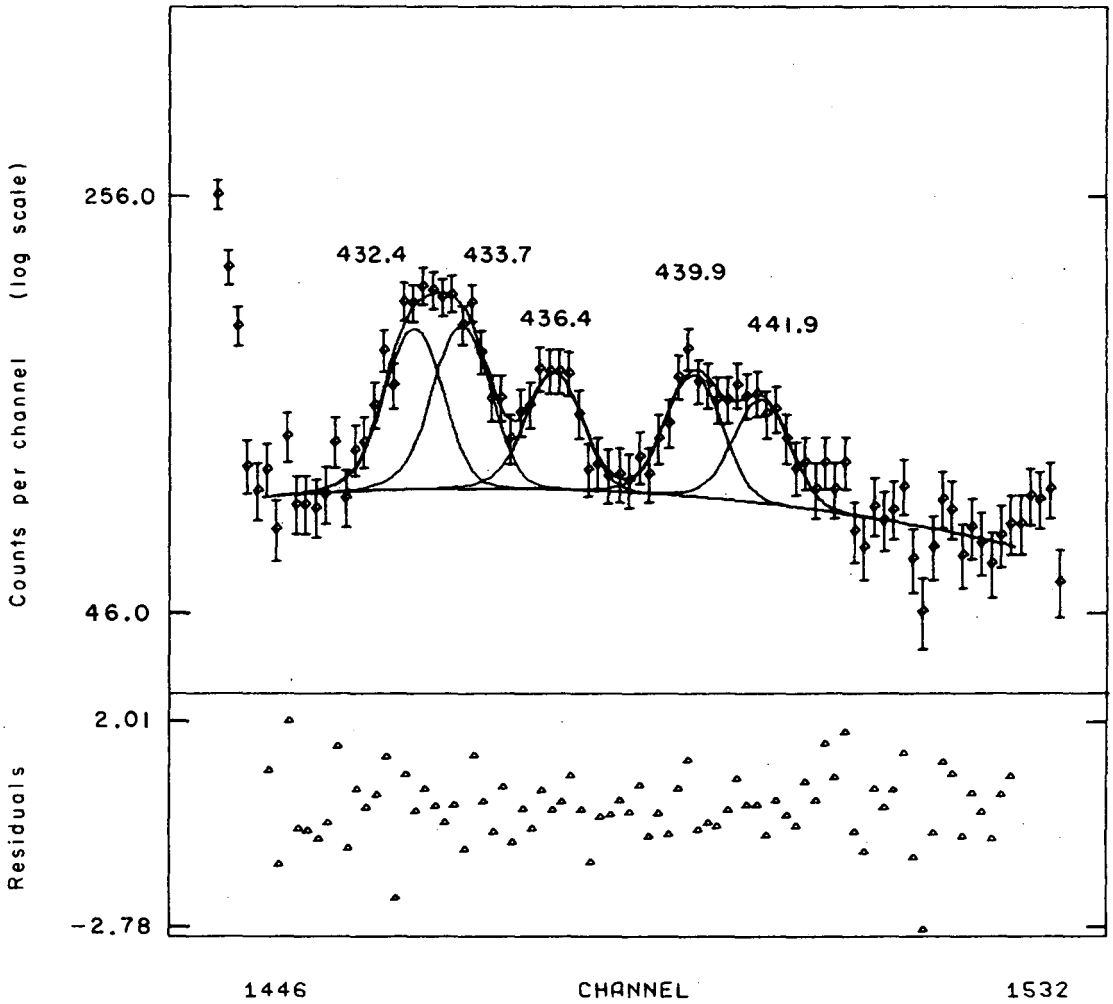
Counts per channel (log scale)
256.0
46.0
432.4
433.7
436.4
439.9
441.9
Residuals
2.01
-2.78
1446
CHANNEL
1532
XBL670-5369-A

Fig. 5

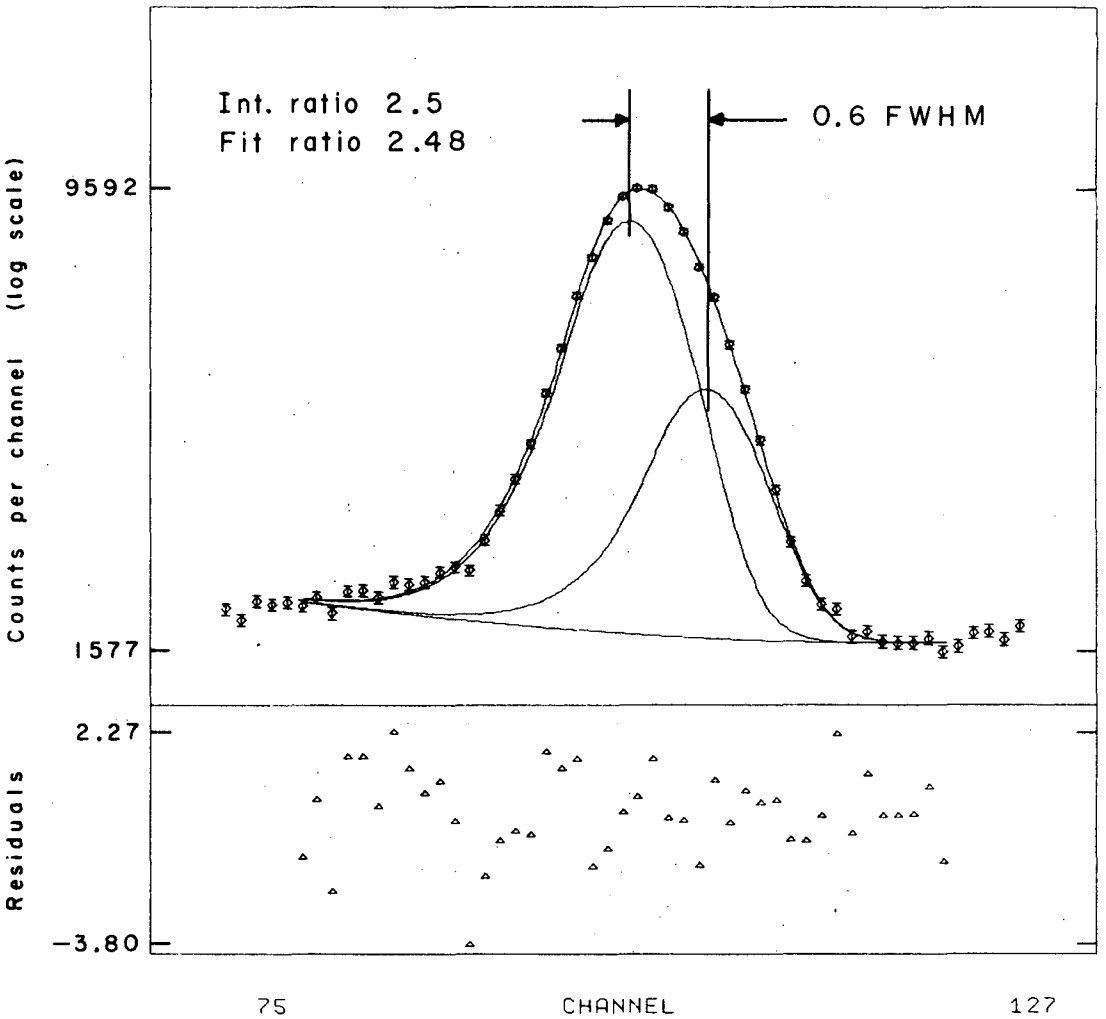

Fig. 6

XBL 6710-2142-A

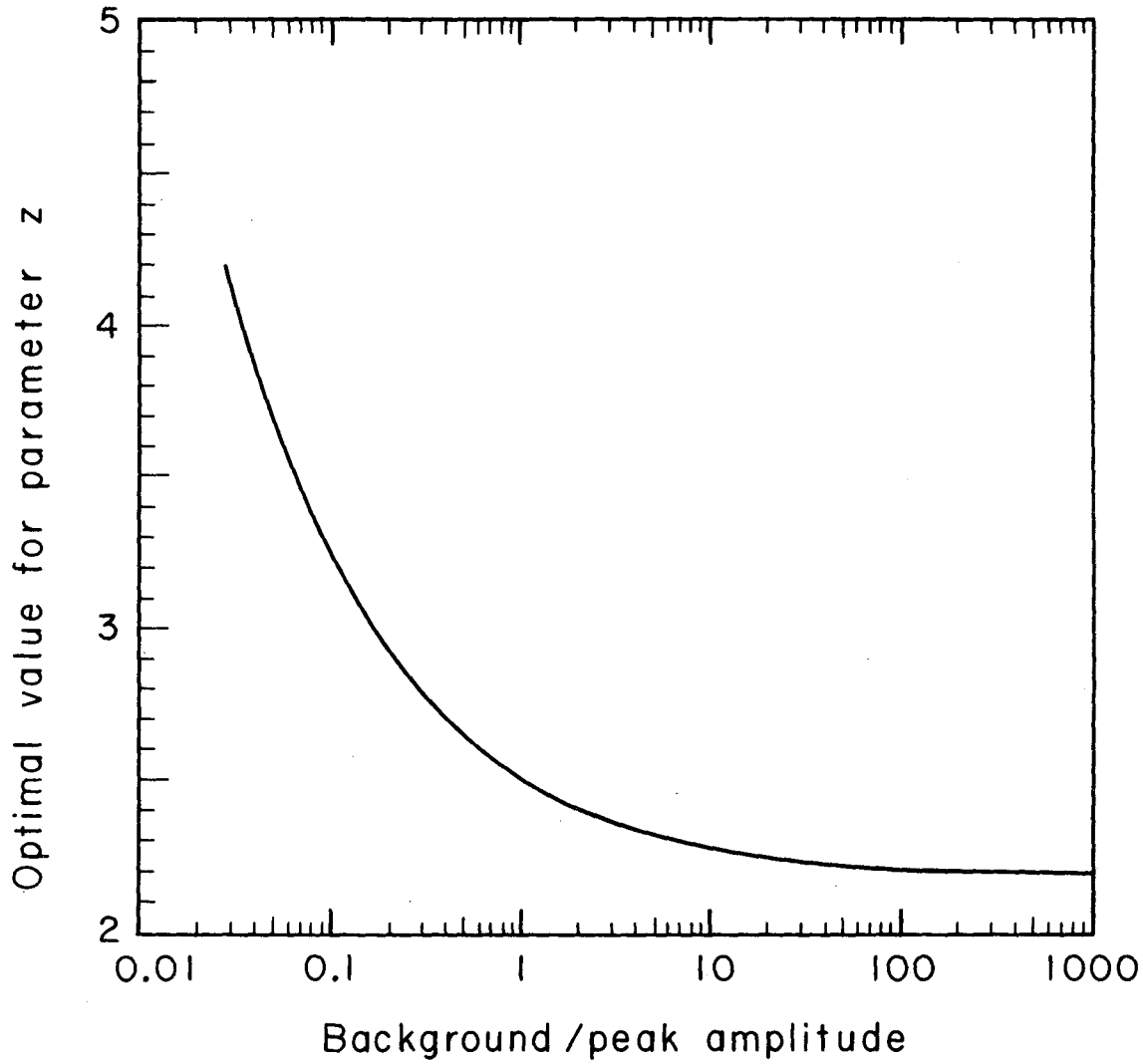

Fig. 7

XBL691-1623

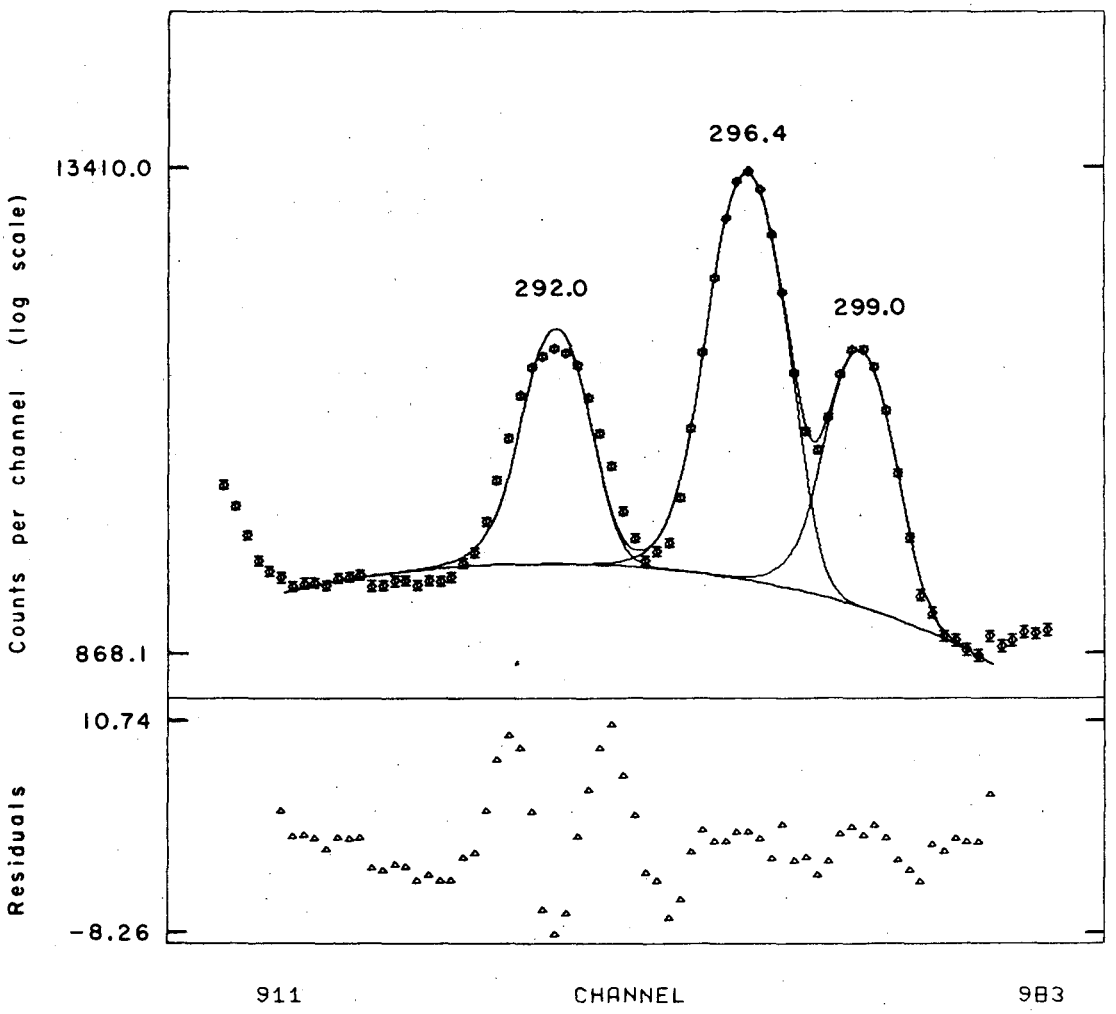
296.4
292.0
299.0
13410.0
868.1
Counts per channel (log scale)
10.74
-8.26
Residuals
911
CHANNEL
983
XBL670-5372-A

Fig. 8

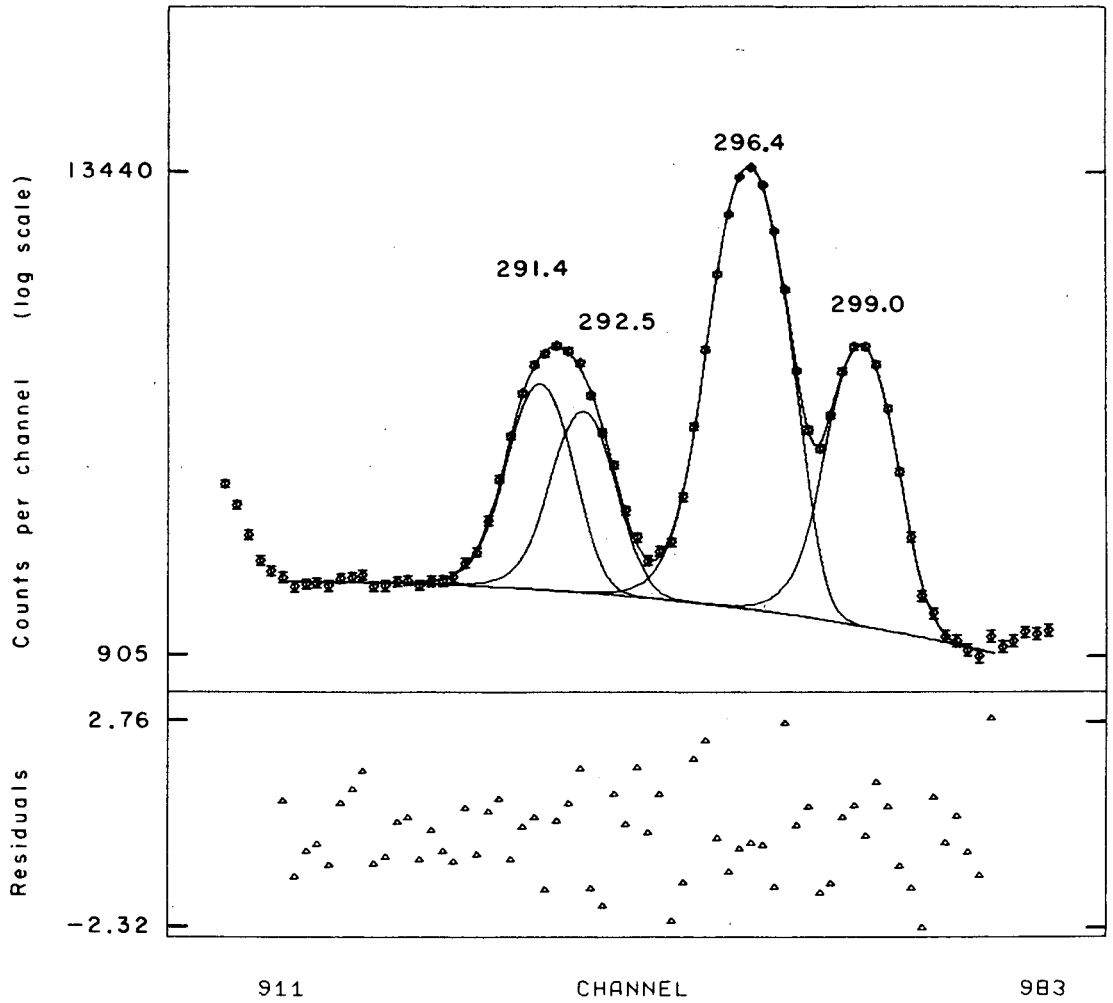

Fig. 9

XBL670-5371-A

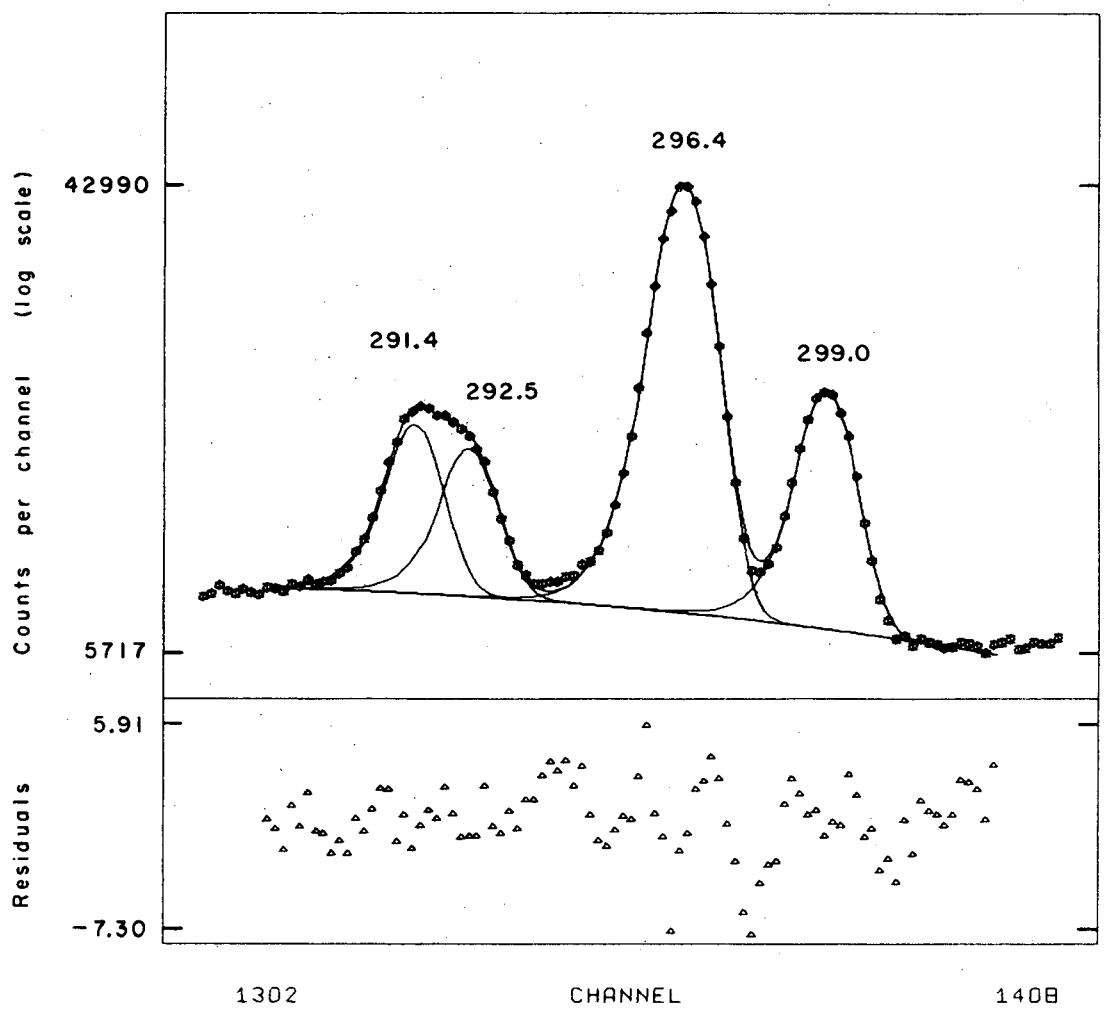

Fig. 10

XBL670-5370-A

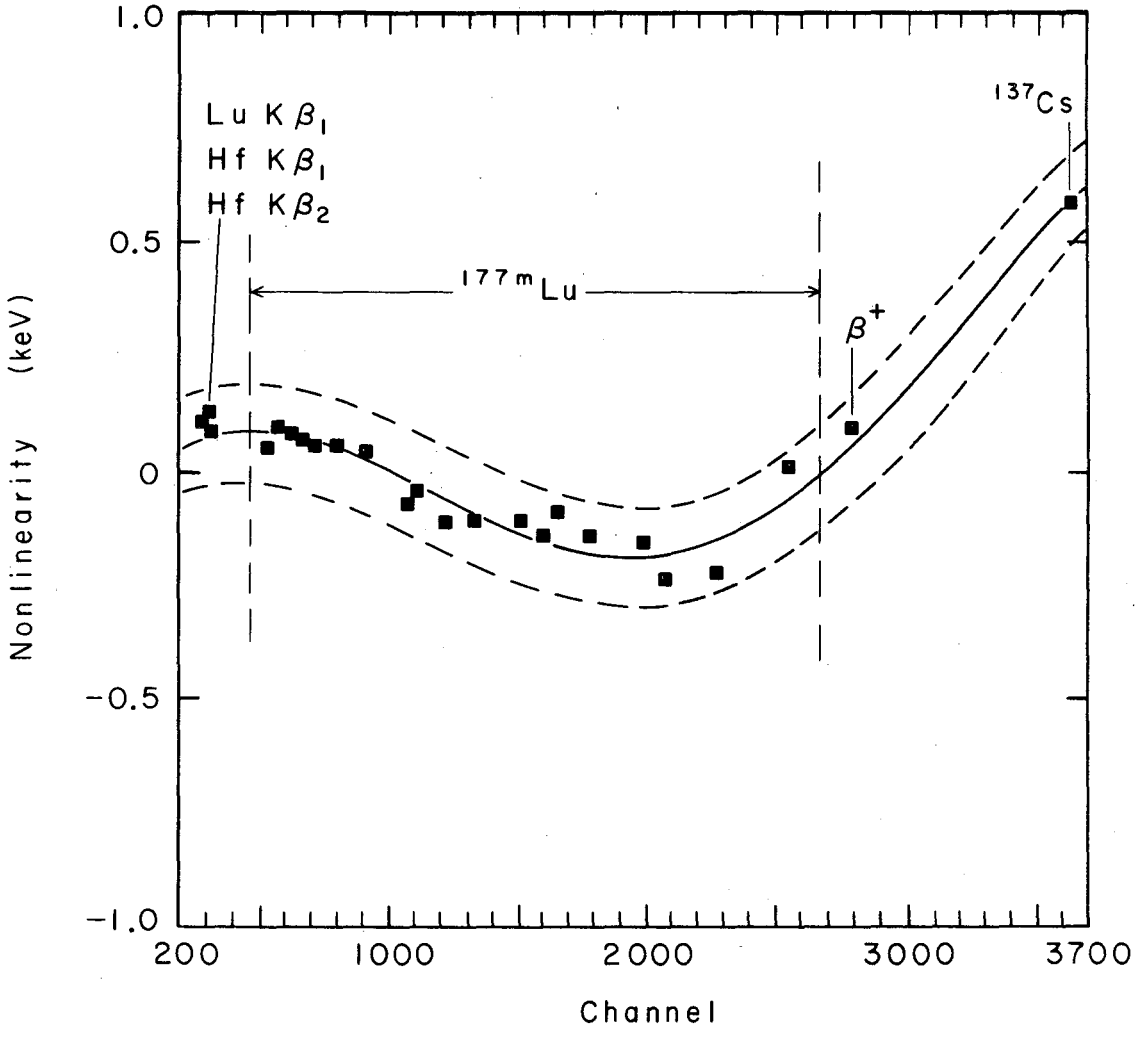

Fig. 11

XBL691-1621

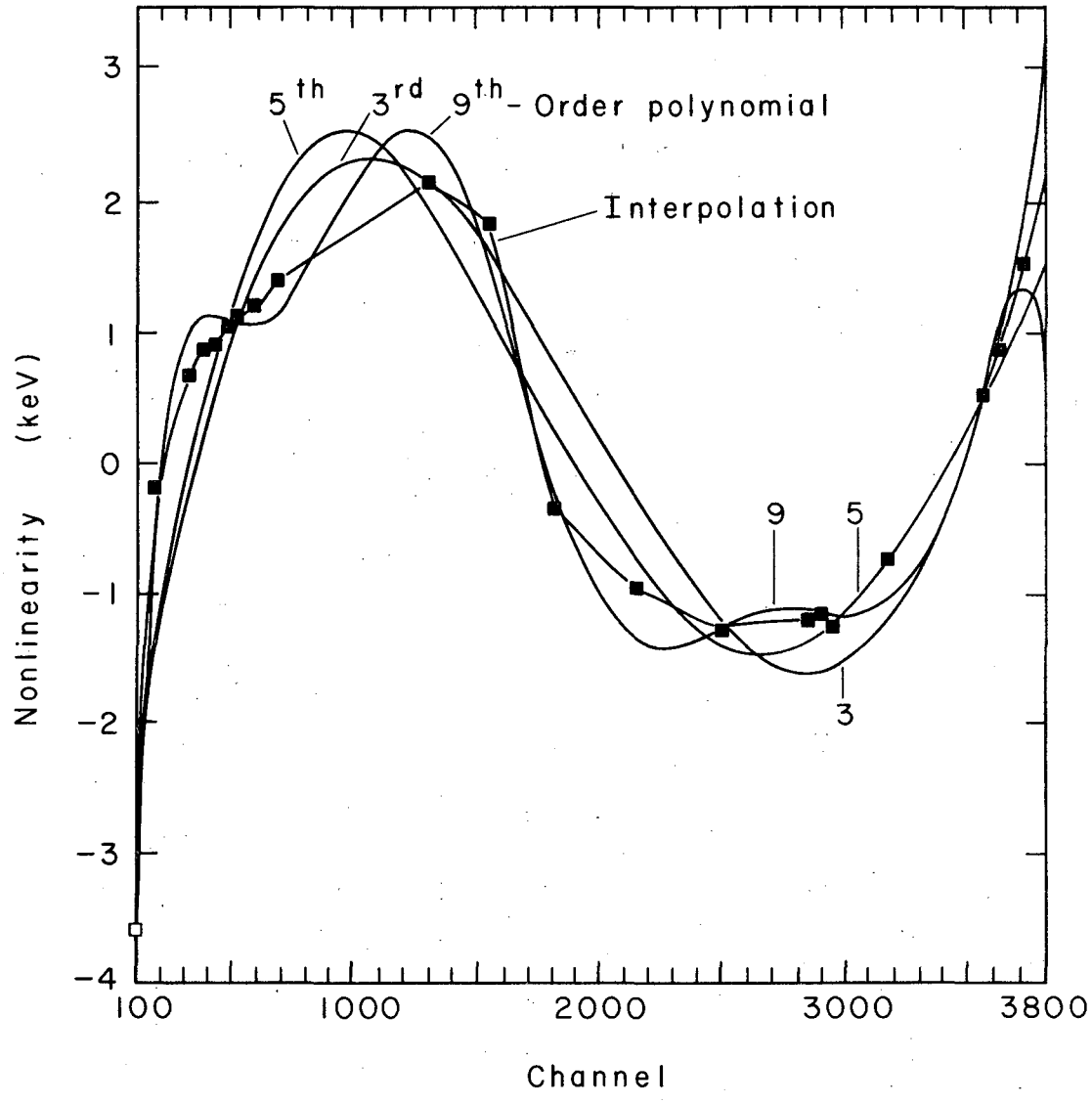

Fig. 12

XBL691-1622

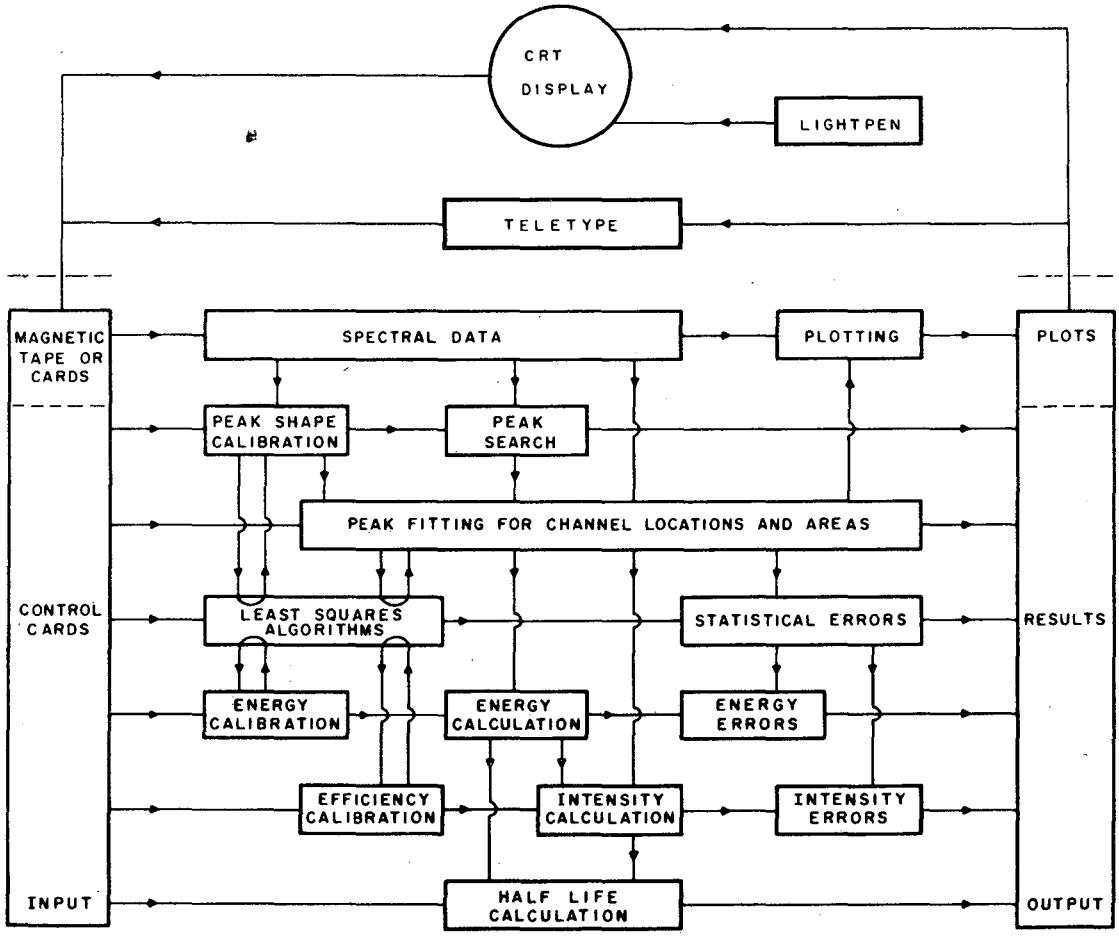

BLOCK DIAGRAM OF PROGRAM SAMPO

XBL670-5375-A

Fig. 13

LEGAL NOTICE

TECHNICAL INFORMATION DIVISION
LAWRENCE RADIATION LABORATORY
UNIVERSITY OF CALIFORNIA
BERKELEY, CALIFORNIA 94720